Environmental Science: Atmospheres

ROYAL SOCIETY OF CHEMISTRY

PAPER

View Article Online
View Journal | View Issue

Cite this: *Environ. Sci.: Atmos.*, 2025, **5**, 1195

Secondary organic aerosol formation from early-generation oxidation products of decamethylcyclopentasiloxane depends on seed aerosol composition

Hanalei R. Lewine, [a] Jeewani N. Meepage, [b] Josie K. Welker, [b] Charles O. Stanier, [c] Elizabeth A. Stone *[bc] and Eleanor C. Browne *[a]

Decamethylcyclopentasiloxane (D_5), a widely used component of personal care products, readily partitions to the atmosphere where it can undergo oxidation, potentially forming secondary organic aerosol (SOA). The mechanism of aerosol formation, particularly at low OH exposure, remains highly uncertain, leaving open questions about the role of multigenerational chemistry, seed aerosol, and oxidation conditions. We performed chamber experiments of D_5 oxidation at low OH exposure to investigate SOA formation from D_5 (SiSOA) and the effect of seed aerosol using dry ammonium sulfate (AS) and dioctyl sebacate (DOS) seeds. We measured gas-phase D_5 and its oxidation products online using chemical ionization mass spectrometry and aerosol size and composition using scanning mobility particle sizing and aerosol mass spectrometry. In select experiments, gas- and particle-phase samples were collected for offline analysis by liquid chromatography with negative electrospray ionization and high-resolution mass spectrometry. The gas-phase products were similar for all experiments, composed primarily of 1-hydroxynonamethylcyclopentasiloxane, a first-generation oxidation product. For AS, the SiSOA was dominated by 1-hydroxynonamethylcyclopentasiloxane, with minor contributions from later-generation products. For DOS, the aerosol was composed of 1-hydroxynonamethylcyclopentasiloxane and an additional unidentified product, and the SiSOA yield was ~3–10 times more than in AS experiments. For AS-seeded experiments, the timeseries of SiSOA evolution throughout the experiment suggests adsorption as the dominant partitioning mechanism, while for DOS-seeded experiments, absorption appears to be important. We estimated the saturation mass concentration (C^*) of the SiSOA to be 1300 μg m^{-3}. Overall, our work shows that the SiSOA formation mechanism depends on seed identity and that multiple oxidation steps will be required for significant SiSOA formation.

Received 29th May 2025
Accepted 19th September 2025

DOI: 10.1039/d5ea00063g

rsc.li/esatmospheres

Environmental significance

Decamethylcyclopentasiloxane (D_5) has been proposed for nomination as a persistent organic pollutant under the Stockholm Convention, thus understanding its environmental fate is important for policy. D_5 is oxidized in the atmosphere to form products that potentially form secondary organic aerosol (SiSOA), but the mechanisms through which SiSOA forms are highly uncertain. We simulated atmospheric chemistry in the laboratory using an environmental chamber to investigate SiSOA formation. We found that SiSOA formation is dependent on the type of seed aerosol present in the chamber. Our results have implications for long-range transport of D_5 and its oxidation products.

Introduction

Cyclic volatile methyl siloxanes (cVMS) are a class of anthropogenic organosilicon molecules that are characterized by a cyclic silicon-oxygen backbone. They are used in numerous applications including as anti-foaming agents, lubricants, precursors for silicon polymers, and in personal care products.[1,2] Decamethylcyclopentasiloxane ($C_{10}H_{30}O_5Si_5$, D_5) is the predominant cVMS used in personal care products and is emitted to the atmosphere at higher rates than other cVMS.[3,4] Emissions in New York City, USA were estimated to be 135 mg per capita per day, while global modeling emission estimates have used a value of 0.05 *Tg* per year for global D_5 emissions.[5–7] Because of its low water solubility and high vapor pressure, ~90% of the D_5 used in cosmetics is estimated to be released to the atmosphere.[3] Emissions of D_5 are centered in urban

[a]*Department of Chemistry and Cooperative Institute for Research in Environmental Sciences, University of Colorado, Boulder, Colorado 80309, USA. E-mail: eleanor.browne@colorado.edu*

[b]*Department of Chemistry, University of Iowa, Iowa City, Iowa 52242, USA. E-mail: betsy-stone@uiowa.edu*

[c]*Department of Chemical and Biochemical Engineering, University of Iowa, Iowa City, Iowa 52242, USA*

areas,[8–10] thus the chemistry in this part of the atmosphere is important for its lifecycle in the environment. Outdoor concentrations of D_5 in densely populated cities are typically in the hundreds of ng m^{-3}.[5,7] cVMS have recently come under scrutiny for being potentially toxic and bioaccumulative,[11–13] and for these reasons in 2023 the European Chemicals Agency proposed to nominate three cVMS, including D_5, for listing as persistent organic pollutants under the Stockholm Convention.[14] This proposed regulation highlights the importance of understanding the environmental fate of D_5, as it could have implications for both environmental health and policy.

The main loss pathway of D_5 is oxidation by OH radicals.[15] D_5 has a lifetime of 4–5 days (24 h average OH concentration of 1.2×10^6 molecules cm^{-3}).[16] Alton and Browne[17] showed that the identity and relative abundances of the initial oxidation products of D_5 is largely independent of peroxy radical (RO_2) fate with the dominant first-generation oxidation product being 1-hydroxynonamethylcyclopentasiloxane, in which one methyl group is replaced by a hydroxyl group (Chart S1).[17] For simplicity, we will refer to 1-hydroxynonamethcylcopentsiloxane as the siloxanol product. In previous studies it has also been referred to as D_4TOH. Subsequent oxidation of the siloxanol is expected to result in the disiloxanol (a second-generation product), where two methyl groups are replaced by hydroxyl groups (Chart S1). The siloxanol has been observed in both ambient aerosol and laboratory D_5-derived SOA (SiSOA) particles.[18–20] Latimer *et al.*[21] studied the effects of different seed types on the partitioning of the siloxanol and found that it remained almost entirely (>99%) in the gas-phase at room temperature and 50% relative humidity (RH) when particles from wood, coal, or diesel combustion were used (at 100 μg m^{-3} aerosol loading).[21] However, in the presence of Arizona test dust (25 °C, 50% RH, 100 μg m^{-3} dust loading), ~33% of the siloxanol was in the particle-phase.[21] This greater affinity for the dust particles was attributed to interactions between the siloxanol and silicon atoms on the dust surface.[21] Inorganic salt seed particles, which represent a substantial portion of ambient aerosol mass,[22] were not investigated.

Recent work has largely focused on understanding SiSOA formation from an absorptive partitioning framework, and has found SiSOA yields ranging between 0% and 150%, increasing as a function of OH exposure with typical exposures ranging from 3×10^{10} to 8.2×10^{12} molecules s cm^{-3} (equivalent to 7 h to 79 days).[23–28] In experiments with significant yields, the major species observed in the aerosol were multifunctional VMS oxidation products (oVMS).[24,25,28–30] This suggested that multiple generations of gas-phase chemistry are required to lower the oVMS volatility enough to form SOA. The idea that multigenerational chemistry is required for significant SiSOA formation is further supported by the need for a gas-phase aging parameter for volatility basis set (VBS) modeling to reproduce yields at high OH exposures.[27] However, there are questions about the atmospheric relevance of the yields measured at high OH exposures. Given the slow oxidation chemistry of D_5, a challenge of these experiments is that achieving high oxidant exposures has required high OH concentrations. These high concentrations can result in the dominance of the RO_2 + OH loss pathway, which is unlikely to be relevant in the ambient atmosphere.[31] Without measuring the gas-phase chemistry concurrently with SiSOA formation, these hypotheses about multigenerational chemistry, RO_2 fate, and seed dependence are difficult to test.

To address knowledge gaps relating to the atmospheric relevance of gas-phase chemistry in SiSOA experiments and adsorption of oVMS to inorganic salts, we performed environmental chamber experiments of D_5 oxidation at OH exposures ~10^{11} molecules s cm^{-3} (~1 day) to investigate the evolution of SiSOA at early generations of oxidation. We used ammonium sulfate (AS) and dioctyl sebacate (DOS) seed aerosol and carefully controlled conditions such that RO_2 primarily reacted with HO_2, conditions which are likely to be important in the ambient atmosphere given the several-day lifetime of D_5. We measured the gas-phase products of D_5 oxidation using toluene chemical ionization mass spectrometry (CIMS) and aerosol products using aerosol mass spectrometry (AMS) in real-time. We characterized particulate (PM) and semi-volatile products by ultra performance liquid chromatography-tandem mass spectrometry (UPLC-MS/MS) offline.

Experimental

Chamber facility

Experiments were performed in a 19.8 m^3 fluorinated ethylene propylene Teflon environmental chamber in the CU Boulder Environmental Chamber facility.[32] Specific conditions for each experiment are summarized in Table 1. All experiments were performed at ambient lab pressure (~860 mbar), low relative humidity (<1%), ~22–24 °C, and with low NO_x. We chose to do experiments under dry and low NO_x conditions to compare to previous chamber experiments.[26] Prior to each experiment, the chamber was flushed with zero air (AADCO model ZA-737-250) overnight. Experiments were run in batch mode, where the chamber was slowly collapsed as air was withdrawn from it.

For all but one experiment, either AS or DOS seed aerosol were added to the chamber. Ammonium sulfate was added by atomizing a 1 or 2 g L^{-1} AS (99.0%, Sigma-Aldrich) solution using a Collision atomizer (TSI model 3076). The seed aerosol flowed through a drier and a charge neutralizer (TSI model 3077) into the chamber until the desired surface area (Table 1) was reached. DOS (97%, Acros Organics) seed was added to the chamber using an evaporation/condensation apparatus. Briefly, an aliquot of DOS was added to a glass bulb which was heated to 200 °C. Zero air was passed over the headspace of the bulb at 0.7 SLPM, which was then diluted into a 4.1 SLPM stream of room-temperature zero air and transported into the chamber.

D_5 (97%, Thermo Fisher, 6 or 14 μL) and hydrogen peroxide (H_2O_2; 30%, Fisher Scientific, 205 μL) were measured using microliter syringes. They were added to the chamber in sequence using a gently heated glass bulb with a stream of N_2 over the headspace. All chemicals were used as received without further purification.

A Teflon-coated fan installed in the chamber was run for 1 minute following each injection. After all injections were complete, the chamber was filled to its full volume at 4 Pa above ambient pressure (~860 mbar) with zero air and allowed to

Table 1 Experimental conditions

Label	Date	Seed; initial surface area (μm^2 cm^{-3})	$[D_5]_0$ (ppb_v)	Chamber temperature (°C)	Oxidation time (h)	Gas-phase oVMS[c] [ppb_v] [μg m^{-3}]	OH_{exp}[c] (molecules s cm^{-3}) $\times 10^{11}$	SiSOA growth[a] (μg m^{-3})	Unique instrumentation[b]
E1	8.08.2023	None	76	21.7	2	10.3 [132.8]	0.71	0	NO_x, QFF, PUF
E2	8.09.2023	AS; 540	57	22.7	2	9.6 [123.7]	0.89	n/a	NO_x, QFF, PUF
E3	8.10.2023	AS; 880	76	21.5	4.9	27.2 [351.9]	2.2	n/a	NO_x, QFF, PUF
E4[d]	8.17.2023	AS; 390	52	22–32	2.9	13.3 [171.6]	1.4	0.46	AMS, QFF, PUF
E5	7.08.2024	AS; 950	55	24.2	2	14.3 [186.6]	1.5	1.07	AMS
E6	7.09.2024	AS; 470	62	24.4	1.8	16.4 [214.6]	1.5	0.62	AMS
E7	7.10.2024	AS; 570	27	24.3	2	5.9 [77.6]	1.2	0.82	AMS
E8	7.11.2024	AS; 900	46	24.5	2	11.0 [143.0]	1.3	1.27	AMS
E9	8.15.2023	DOS; 1300	61	22.6	1.7	5.6 [72.4]	0.46	1.68	AMS
E10	8.16.2023	DOS; 750	67	22	5	15.0 [195.4]	1.2	5.76	AMS
E11	7.12.2024	DOS; 1700	0	24.5	2.5	0.2 [2.73]	n/a[e]	0.046	AMS

[a] SiSOA growth is calculated from AMS measurements. [b] All experiments used CIMS and SMPS. [c] oVMS and OH exposure are likely overestimated because of the assumptions used to calculate oVMS. Based on the amount of injected H_2O_2, H_2O_2 was 3 ppm_v for all experiments. [d] During E4 the air handler failed. During the first 1.5 h of oxidation the temperature was 22 °C, then it increased to 32 °C over the next hour. [e] No D_5 was injected so the OH exposure cannot be determined.

equilibrate for 30–45 minutes. Blacklights (Osram/Sylvania model F40/350BL/ECO and Osram model FR48T12/350BL/VHO/180, peak wavelengths 360, 404, 436, 545, 577 nm) were then turned on to initiate photochemistry. Oxidation proceeded for 2–5 hours (Table 1), then the lights were turned off and in experiments 1–4 (E1–E4) the filter samples were collected (described in the sample collection section). During select experiments, there were two periods with lights on to investigate stability of oVMS and SiSOA. For E11, we only injected DOS and H_2O_2 to investigate DOS oxidation by OH. In E1–E4 and E9–E10, when the pressure within the chamber reached ambient pressure ~3 h after filling the bag, the top of the chamber bag was lowered to maintain a positive pressure in the chamber.

Online measurements

Temperature and relative humidity were monitored in the chamber using Vaisala probes (HMP110 and HMP60). NO and NO_2 (NO_x) were measured in select experiments using a chemiluminescence NO and NO_2 analyzer with a blue light converter for true NO_2 measurements (Teledyne, T200UP) with 1 min resolution and 50 ppt_v limit of detection for NO and NO_2.

A scanning particle mobility sizer (SMPS; TSI models 3080 electrostatic classifier, 3081 differential mobility analyzer, and 3010 condensation particle counter) was used to measure particle number and size distributions.

A high-resolution time-of-flight aerosol mass spectrometer (HR-ToF-AMS, Aerodyne, Inc.) was used in select experiments to characterize aerosol chemical composition.[33] AMS measurements were analyzed with ToF-AMS analysis software (Squirrel version 1.66 G and PIKA version 1.26 G) in Igor Pro (version 9.05, Wavemetrics). The specific version of the code included the fix for isotopologue intensity calculation that is included in version 1.27 of PIKA. We performed high resolution (HR) peak fitting below m/z 100 for AS and 107 for DOS. Above these values we use only unit mass resolution data due to limited resolving power. A relative ionization efficiency (RIE) of 1.2 was used for sulfate. A RIE of 1 was used for SiSOA. The RIE for SiSOA is likely different from 1, but we are unable to constrain it due to the low yields. Although the absolute amount of SiSOA may not be accurate, relative changes between experiments can be compared because we expect the RIE for SiSOA to be essentially constant. For AS experiments, SiSOA was corrected for wall loss and collection efficiency by normalizing to the initial AS loading (determined by the SMPS). In DOS experiments the collection efficiency was assumed to be 1 due to the liquid nature of the aerosols. Inspection of DOS tracer ions shows that oxidation of DOS was occurring, but there is no evidence for a change in the collection efficiency. No wall loss correction was applied for the DOS experiments due to substantial uncertainty as discussed in the SiSOA formation and composition in DOS-seeded experiments section. Only AMS measurements were used to calculate SiSOA growth because the volume growth was too small to see using SMPS.

Gas-phase D_5 and its oxidation products were measured in real-time using a High-Resolution Chemical Ionization long time-of-flight Mass Spectrometer (CIMS, Tofwerk AG and

Aerodyne, Inc.) sampling from the chamber. As in our previous work, we used protonated toluene as the reagent ion.[16,17] Ionization by toluene is soft; we do not detect the fragment resulting from methane loss from D_5 or its oxidation products. All compounds were detected as $[M + H]^+$ ions. Mass spectra were analyzed using Tofware v3.3.0 in Igor Pro using fully constrained peak fitting. Reported signal intensities are for the monoisotopic ion. Signals were duty-cycle corrected at *m*/*z* 92 and normalized to the toluene signal ($C_7H_8^+$). We did not apply a transmission correction.

Silicon's unique and prominent isotopic signature (^{28}Si 92.2%, ^{29}Si 4.7%, ^{30}Si 3.1%)[34] creates a distinctive pattern that aids in identifying Si-containing species, however it complicates assigning isobaric oVMS ions. The monoisotopic protonated D_5 ion ($(C_{10}H_{30}O_5[^{28}Si]_5)H^+$) appears at *m*/*z* 371.101, and its ^{30}Si isotopologue ($(C_{10}H_{30}O_5[^{28}Si]_4[^{30}Si])H^+$, *m*/*z* 373.098) has a relative abundance of 23.85%. The protonated siloxanol ion ($(C_9H_{28}O_6Si_5)H^+$, *m*/*z* 373.081) was unresolved from the D_5 isotopologue at the same unit mass because insufficient D_5 reacted away for us to fit the siloxanol signal. Consequently, signal attributed to the siloxanol is calculated by subtracting the ^{30}Si isotopologue of D_5 from the unit mass integrated *m*/*z* 373 signal.

An unidentified background source of D_5 prohibited us from fully quantifying the amount of D_5 reacted, OH exposure, and SOA yield. When the lights were on, the measured D_5 decay was more variable than anticipated and even increased during oxidation during E4, E8, E9, and E10 (Fig. S1). Additionally, in E5–E8, less D_5 appeared to react (~4% in E5–E8 *vs.* ~12% in E1–E4 and E9–10) despite similar experimental conditions. The absolute signal increase in oVMS was similar between all experiments, so this difference in apparent decay may be due to the background D_5. Before starting an experiment, D_5 in the chamber was always < 1 ppb_v, which was inconsistent with the unidentified source. We investigated various explanations for the background such as wall loss,[35,36] off-gassing, and tubing effects (Fig. S2), however none of these effects could fully explain the measurements. A detailed description is in Text S1 in the SI.

Due to the unknown background source, we were unable to use the decay of D_5 to estimate OH exposure. To estimate OH exposure, we instead used the oVMS signal. This approach is possible due to the low SiSOA yield and the negligible wall loss of these compounds. oVMS were estimated using experiment E1 in which no SiSOA was formed. In E1, it was assumed that all reacted D_5 in ppb_v was converted to the siloxanol, formate ester, and $C_{10}H_{30}O_8Si_5$ products in the gas-phase. This mass balance approach was used to obtain a calibration factor for oVMS since authentic standards are unavailable. The factor was assumed to be the same for all species and the same factor was used in all experiments. Because the distribution of oVMS products varied minimally between the different experiments (discussed in detail in the Gas-phase oxidation chemistry section), this approach is appropriate for providing an estimate of the OH exposure. The CIMS was calibrated for D_5 by passing N_2 over a perm tube containing liquid D_5 that was held at 30 °C.

OH exposure in molecules s cm^{-3} was calculated as

$$OH_{exp} = -\ln\left(\frac{D_{5_0} - oVMS_{end}}{D_{5_0}}\right) \Big/ k_{OH} \quad (1)$$

where k_{OH} = 2.1 × 10^{-12} cm^3 $molecules^{-1}$ s^{-1}.[16] Using a temperature dependent rate coefficient determined by Bernard and Burkholder[37] would result in variations in k_{OH} of 2.7% across the temperature range of our experiments (Table 1). The OH concentration in molecules cm^{-3} was calculated by dividing the OH exposure by the oxidation time in seconds.

D_4 ($C_8H_{24}O_4Si_4$) and D_6 ($C_{12}H_{36}O_6Si_6$) were both detected after D_5 was injected into the chamber at an average relative abundance of 100 : 0.09 : 1.5 D_5 : D_4 : D_6 signal ratio, suggesting that D_4 and D_6 likely originate from impurities in the D_5.

Offline measurements

Sample collection. In E1–E4, aerosol and semi-volatile samples were collected for offline analysis using a two-stage filter holder. In the first stage, PM was collected onto precleaned (550 °C for 18 hours)[19] quartz fiber filters (QFF, 47 mm, PALL Life Sciences). Semi-volatile gases were collected onto precleaned polyurethane foam filters (PUF; URG-2000-30-52PC). Air was drawn from the chamber at a flow rate of 20 L min^{-1}. Sampling flow rates were continuously measured with a calibrated rotameter to ensure consistency. Air samples were collected after lights were turned off over a period of 3 hours, resulting in the sampling of 3.6 m^3 of air, corresponding to approximately 18% of the chamber's total volume.

PM samples were prepared for chemical analysis as described in Meepage *et al.*[19] Briefly, portions of filters (8.63 cm^2 for qualitative analysis and 0.117 cm^2 for semiquantitative analysis) were extracted twice sequentially by sonication (30 minutes each, 60 sonics per min) with acetonitrile and ultrapure water (95 : 5, 10 mL). The combined extracts were filtered through polypropylene membrane syringe filters (0.45 μm followed by 0.20 μm pore size, Puradisc, Whatman), and the volumes were reduced to 500 μL under a stream of ultra-high purity nitrogen gas (≤5 psi) at 50 °C using a Turbovap LV evaporation system (Caliper Life Sciences).

The extracts were transferred to LC vials (1.5 mL, Agilent) and evaporated to near dryness (50 μL) under a very light stream of ultra-high purity nitrogen gas at 50 °C using a microscale nitrogen evaporation system (ReactiTherm III TS 18824 and Reacti-Vap I 18825, Thermo Scientific). They were then reconstituted in 180 μL of acetonitrile : ultra-pure water (95 : 5). Finally, 20 μL of 1000 μg L^{-1} D_5–phenol was added as an injection internal standard to bring the final volume to 200 μL.

Semi-volatile samples were prepared for chemical analysis as described in Al-Naiema and Stone.[38] Briefly, PUF filters were extracted by three sequential compressions using acetonitrile. The combined extracts were evaporated to 1 mL by rotary evaporation at 30 °C (120 rpm, 200 mbar). The reduced extracts were filtered with a regenerated cellulose syringe filter (0.2 μm, Whatman™) and evaporated to 250 μL under a gentle stream of ultra-pure nitrogen at 30 °C using a microscale nitrogen evaporation system (ReactiTherm III TS 18824 and Reacti-Vap I 18825, Thermo Scientific). One field blank, collected under the same handling protocols as the samples but without active

airflow, was analyzed by the UPLC-MS/MS method described below; no oVMS were detected except the D_5-derived siloxanol, whose QFF field-blank signal was 2.6 orders of magnitude lower than the average siloxanol concentration measured in the AS-seeded experiments.

UPLC-MS/MS data collection and analysis. An ultra performance liquid chromatograph (UPLC) coupled to a Q-Exactive Quadrupole Orbitrap mass spectrometer (Thermo Scientific) was used in negative mode with a heated electrospray ionization source, following the conditions described in Meepage *et al.*[19] Separation was performed on a reversed-phase BEH C-18 column (2.1 × 100 mm, 1.7 μm, Premier ACQUITY UPLC Waters) following the gradient elution, flow rate, and column conditions described by Meepage *et al.*[19] To avoid the potential risk of introducing a high salt concentration of AS in the seeded chamber samples with the solvent front into the mass spectrometer, the eluent was directed to the waste stream for the first minute, after which data collection started.

The optimized ionization conditions, utilizing an acetonitrile–water solvent system and a 10 mM ammonium bicarbonate-ammonium hydroxide buffer at pH 10, provided sensitive and reproducible measurements of siloxanol functional groups in the *m*/*z* range of D_5. However, this ionization method is insensitive toward silyl methanol functional groups due to their lower acidity. Additionally, this method is unable to detect formate esters and ether peroxides, either because of their low ionization efficiency and/or loss during sample preparation. Because of the unavailability of authentic standards for quantitation, relative product distributions were determined assuming equivalent ionization efficiencies. Compared to previous studies that utilized a Q-Exactive Quadrupole Orbitrap mass spectrometer for detecting similar compound classes,[24,29,30] our method separated compounds before detection. This separation provides insight into isomeric distributions and aids in identification of adducts and fragment ions.

Data acquisition was conducted using Xcalibur 4.2 software (Thermo Scientific), while qualitative analysis was performed with Compound Discoverer 3.3.0 (Thermo Scientific). Initially, peaks detected in the field blanks were identified and subtracted. A targeted analysis was developed using 135 compounds identified in previous literature.[24,29] In addition, another targeted approach was applied to account for anticipated structural modifications, such as the substitution of methyl groups with OH or CH_2OH, allowing for up to 10 replacements. Peaks were assigned molecular formulas based on the following criteria: (a) elemental composition falling within the ranges of $C_{0–30}H_{0–90}O_{0–30}Si_{0–20}N_{0–10}S_{0–5}$, (b) theoretical *m*/*z* values within ±5 ppm of the observed *m*/*z*, and (c) isotope distributions of the detected species.

Semi-quantification was carried out with TraceFinder v4.0 (Thermo Scientific) with tris(*tert*-butoxy)silanol (99.999%, Sigma-Aldrich) as an oVMS surrogate standard. The standard curve gradients were set at 4, 38, 379, 946, 1893, 3785 nmol L^{-1} for tris(*tert*-butoxy)silanol, and the linearity of the calibration (R^2) curve was calculated to be 0.9994. D_5–phenol (98%, Sigma-Aldrich) was used as the internal standard.

Modeling

We used KinSim v4.21 [39] to simulate gas-phase chemistry and absorptive partitioning in the chamber and to estimate the RO_2 fate in our experiments. The mechanism is provided in the SI (Tables S1–S4). Rate coefficients for non-D_5 reactions were obtained from Atkinson *et al.*[40,41] The growth of oxidation products in E1 was used to constrain the photolysis rate of H_2O_2, the oxidant precursor. A photolysis rate of 7.4×10^{-6} s^{-1} was used, although we note this is likely overestimated based on how we estimated the oVMS concentration. The D_5 + OH oxidation rate coefficient was obtained from Alton and Browne.[16] The rate coefficients for D_5-derived RO_2 reactions with RO_2, NO, and OH were assumed to be the same as those for non-Si containing RO_2 and were from Ziemann and Atkinson[42] for RO_2 + RO_2 and RO_2 + NO, and from Fittschen[43] for RO_2 + OH. The rate coefficients for D_5-derived RO_2 unimolecular reactions and the reaction with HO_2 were from Alton *et al.*[44] As the k_{OH} of later-generation oVMS have not been measured, and structure–activity relationships have only been developed for the parent compounds, we used the same rate constants for oVMS as for D_5. The model was initiated with 3 ppm H_2O_2, 70 ppt NO, 500 ppt NO_2, the measured mixing ratio of D_5, and, in cases with partitioning, the background organic aerosol (OA) concentration measured by the AMS, or, for DOS cases, the calculated mass derived from the SMPS. We used the estimated oVMS mixing ratio in each experiment to constrain the model.

Gas-wall partitioning calculations were not included because gas-wall partitioning for D_5 and the first-generation oVMS is expected to be unimportant based on the estimated C^* from the tubing-delay experiment (Text S1). Absorptive partitioning was calculated for first-generation oxidation products using the C^* of 50 000 μg m^{-3} (based on the siloxanol C^*) and second-generation products using a C^* of 2600 μg m^{-3}.[17] We also calculated a C^* value for the SiSOA formed in the DOS experiments and used that to model the AS experiments.

We model adsorptive partitioning as a reversible process as in Pöschl *et al.*[45,46] From gas kinetic theory, the collision flux of gas molecules of species X_i with a surface per unit time is calculated as:

$$J_{\mathrm{coll},X_i} = [X_i]_{gs}\omega_{X_i}/4 \quad (2)$$

where $[X_i]_{gs}$ is the concentration of X_i in the gas-phase close to the surface and ω_{X_i} is the mean thermal velocity of X_i. $[X_i]_{gs}$ will differ from the average gas-phase concentration of X_i ($[X_i]_g$) due to mass transport limitations that depend on the flow regime. Due to the approximate nature of the calculation as well as the fact that quantities such as the diffusion coefficients of the relevant species are unknown, we approximate $[X_i]_{gs}$ as equal to $[X_i]_g$. We calculate that this approximation alters our results by only ~7%.

The flux of molecules adsorbing to the particle surface is given by:

$$J_{\mathrm{ads},X_i} = \alpha_{s,X_i} J_{\mathrm{coll},X_i} \quad (3)$$

where α_{s,X_i} is the accommodation coefficient, defined as the probability that X_i does not scatter or react upon collision. The value of α_{s,X_i} will vary over the course of the experiment as sorption sites become occupied. Assuming a Langmuir adsorption model gives:

$$\alpha_{s,X_i} = \alpha_{s,0,X_i}(1 - \theta_s) \quad (4)$$

where $\alpha_{s,0,X_i}$ is the accommodation coefficient on an adsorbent-free surface and θ_s is the fractional surface coverage of all adsorbates. The model considers competitive adsorption of two compounds, the siloxanol (X_1) and the disiloxanol (X_2), but we treat them as having identical physical properties to reduce the number of unknowns. Thus, we can write

$$\theta_s = \frac{\sigma_X([X_1]_s + [X_2]_s)}{A} \quad (5)$$

where $[X_i]_s$ represents the surface concentrations (here given per volume of air to facilitate comparison to the measurements), A is the surface area concentration of the aerosol, and σ_X is the effective cross-section of X. We estimate $\sigma_X \approx 9 \times 10^{-15}$ cm^2 from the density of D_5 (0.959 g cm^{-3})[47] and assuming the siloxanol molecule is a sphere. The same cross-section is used for both the siloxanol and disiloxanol.

Chandramouli and Kamens[20] estimated the rate of desorption (k_{off}) in s^{-1} for the siloxanol as it varies with temperature as given in eqn (6):

$$k_{off} = 3.1623 \times 10^{12}\, e^{-9622/T} \quad (6)$$

Altogether, the change in concentration of adsorbed X_i over time is:

$$\frac{d[X_i]_s}{dt} = \alpha_{s,0,X_i}\left(1 - \frac{\sigma_X([X_1]_s + [X_2]_s)}{A}\right)\frac{\omega_X}{4}[X_i]_g A - k_{off}[X_i]_s \quad (7)$$

In the model we fix ω_X (calculated), A (measured by SMPS), σ_X (estimated), and k_{off} (estimated). For $[X]_g$ we use timeseries of gas-phase concentrations of the siloxanol and disiloxanol output from KinSim simulations of gas-phase chemistry. We use the model to fit $\alpha_{s,0,X_i}$ (described in the modeling section below).

Results and discussion

Gas-phase oxidation chemistry

The goal of our experiments was to probe aerosol formation for the early-generation oxidation products and thus we targeted OH exposures of 10^{10}–10^{11} molecules s cm^{-3} (Table 1). We estimate OH concentrations of 0.68–1.8 $\times 10^7$ molecules cm^{-3}, however this range is likely overestimated due to the uncertainty in the oVMS estimation. Our exposures correspond to 0.1–0.5 D_5 lifetimes (11 h to 2 days) (assuming a 24 h average OH concentration of 1.2×10^6 molecules cm^{-3}). Fig. 1b shows an example CIMS timeseries from an AS-seeded D_5 oxidation experiment (E7) with the D_5 signal and the major oVMS species detected. The observed oxidation products (Chart S1) are consistent with only one oxidation step. Compounds were identified based on past work[16,17] and include $C_9H_{28}O_6Si_5$ identified as the siloxanol, $C_{10}H_{28}O_7Si_5$ assigned as the formate ester, and $C_{10}H_{30}O_8Si_5$. $C_{10}H_{30}O_8Si_5$ has previously been attributed to an ether hydroperoxide,[17] but may also be a trioxide compound. When the lights were turned off, terminating oxidation, the siloxanol accounted for 71–91% of the measured oVMS signal, the formate ester for 8–28%, and $C_{10}H_{30}O_8Si_5$ ~1%. The relative contributions of the major oVMS in each experiment are shown in Fig. S3 and are consistent with past measurements of the signal distribution by our group.[17] As seen by the consistency between E1 and the other experiments, the presence of seed aerosol did not appear to affect the product distribution. In E5–E8 there was more formate ester relative to the siloxanol compared to E1–E4 and E9–E10 (Fig. 1). The reasons for this change are unclear since the predicted RO_2 fate (discussed below) is consistent to within a few percent for each experiment.

We expect the major second-generation oxidation product to be the disiloxanol (Chart S1).[17] The disiloxanol, and any other gas-phase second-generation oxidation products were below the detection limit of the CIMS.

We used KinSim[39] to model the gas-phase oxidation chemistry and to estimate the RO_2 fate in our experiments. Because of the uncertainty in the measured D_5, we used the measured oVMS to constrain the model (Fig. S4–S6). The model results for E1 showed that the RO_2 reacted with HO_2 92% of the time and with NO 6.1% of the time. It isomerized 1.4% of the time, RO_2 + OH was 0.4%, and the remainder was RO_2 + RO_2. The model predicted that ~6% of the gas-phase products were second-generation and ~0.3% were third-generation.

SiSOA formation and composition in AS-seeded experiments

In an unseeded experiment (E1) we observed no nucleation (total SMPS number concentration < 3 cm^{-3}). However, in the presence of ammonium sulfate seed aerosol, small amounts of SiSOA formed. Fig. 2 shows an average background subtracted aerosol mass spectrum of the AS-seeded SiSOA. The most prominent ion is $C_3H_9Si^+$, which has previously been identified as a contaminant from conductive silicon tubing.[48] However, no conductive tubing was used in the AMS sampling inlet and its signal is constant until oxidation is initiated by turning on the lights, indicating that it is a product of D_5 oxidation. We assigned non-Si-containing ions at low mass (CH_3^+, CHO^+, and CH_2O^+) to SiSOA because their signal increased when the lights turned on. The electron ionization (EI) spectrum of D_5 contains ions at the same nominal masses as CH_3^+ and CHO^+,[49] consistent with these ions fragmenting from SiSOA. The high m/z range is dominated by Si-containing ions. The overall mass-spectrum of the SiSOA shows similarities to previous EI spectra of the siloxanol. Chandramouli and Kamens[20] reported the mass spectrum of a siloxanol standard and Milani *et al.*[18] measured the mass spectrum of the siloxanol in an ambient aerosol sample. The spectrum contains characteristic ions at m/z 163, 193, 251, 267, 325, and 341 ($C_7H_{21}O_6Si_5^+$, formed from the loss of two methyl groups). Our SiSOA AMS spectra has prominent ions at the same unit masses. The measured exact mass of

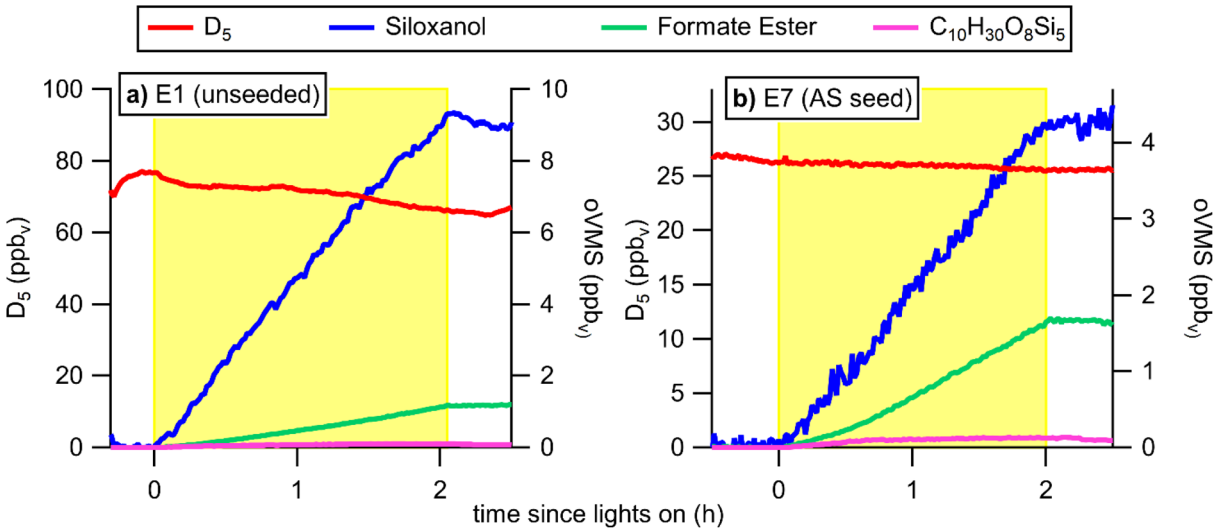

Fig. 1 Example gas-phase CIMS timeseries from experiments (a) E1 and (b) E7. Yellow shading indicates when lights were on and oxidation was occurring. D_5 mixing ratio is shown on the left axes and oVMS are on the right axes. Note that the D_5 timeseries includes potential interference from the unidentified background source of D_5. Signals are averaged to 1 min time resolution.

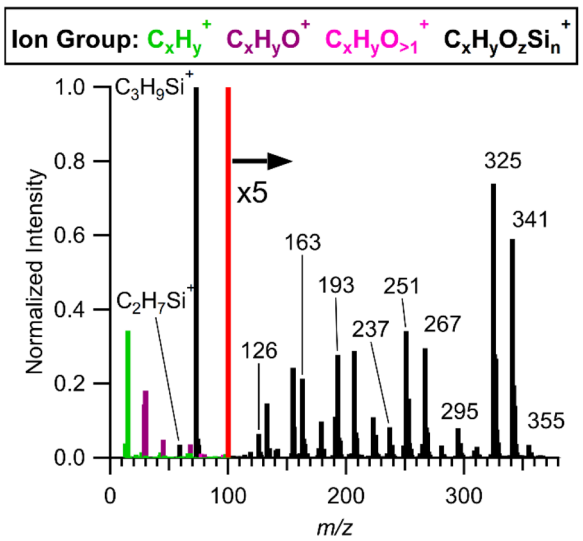

Fig. 2 Background-subtracted average AMS mass spectrum of SiSOA from experiment E7 with AS seed. Spectrum is normalized to a $C_3H_9Si^+$ intensity of 1.

the peak at m/z 341 is consistent with that of $C_7H_{21}O_6Si_5^+$ to within 0.6 ppm and the observed isotope distribution agrees with the theoretical values for $C_7H_{21}O_6Si_5^+$ (Fig. S7). Our spectra differs from Chandramouli and Kamens[20] in that m/z 325 is the most intense peak rather than m/z 341. Other characteristic peaks in our spectra also have different relative intensities than those previously reported. These differences are likely the result of additional species in the SOA and/or fragmentation occurring during vaporization. We also observed a number of doubly charged Si-containing ions in the SiSOA, which are discussed in the SI (Fig. S8 and Text S2). Doubly charged ions formed from electron ionization of D_3 and D_4 siloxanes have been previously observed.[50] Because background at these half-integer masses should be low, they may be of use as tracers for SiSOA in ambient AMS measurements.

Fig. 3 shows the timeseries of SiSOA growth for E7 with AS seed. We were unable to quantify the SiSOA growth using SMPS because uncertainty in SMPS wall loss corrections was greater than the SiSOA growth observed in the AMS. The SiSOA is non-zero before the lights turn on because we do not attempt to apportion the signal of the CHO ions or high mass ions between background organic aerosol and SiSOA. Other background ions

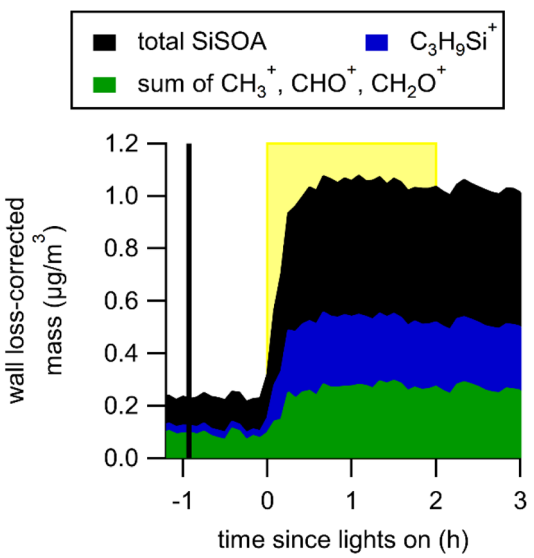

Fig. 3 Example wall loss corrected AMS timeseries of SiSOA growth from experiment E7 with AS seed. Yellow shading indicates when the lights were on and oxidation was occurring. The vertical line indicates when D_5 was injected into the chamber. Measurements are averaged to 5 min time resolution.

do not change in magnitude after oxidation is initiated, so we do not expect the portions of these signals coming from the background to change throughout the experiment. When calculating total SiSOA, we take the difference between the final and initial values. No observable increase in SiSOA occurs following D_5 injection showing that D_5 itself does not partition onto the aerosol. SiSOA begins growing once D_5 oxidation is initiated and reaches a maximum around 30 minutes after the lights turn on. After this, the SiSOA remains constant even after the lights turn off.

When the lights were turned on, we observed a decrease in the AMS sulfate signal of ~10% over the course of ~20 min (Fig. S9). We attribute this to a change in the collection efficiency due to SiSOA accumulating on the AS particles. This decreased collection efficiency is presumably due to increased bounce.[51]

Unlike in the gas-phase, we see evidence for higher-generation oxidation products in the SiSOA. While m/z 325 has been identified as a characteristic fragment ion of the siloxanol,[18,20] m/z 327 has been observed as the more prominent ion in SiSOA in previous lab studies that used AMS to analyze the SiSOA.[25,28,30] Given that the disiloxanol is formed from conversion of a CH_3 group on the siloxanol to an OH group, it could fragment similarly to give ions 2 m/z above the siloxanol fragment ions. Because of silicon's isotopic pattern, the species at m/z 325 has a large contribution to m/z 327. In order to visualize the contribution of the monoisotopic species at m/z 327, we plot the enhancement in the ratio of m/z 327/m/z 325, calculated as:

$$\Delta = \frac{m/z327}{m/z325} - \left(\frac{m/z327}{m/z325}\right)_{i,\mathrm{avg}} \quad (8)$$

where the initial ratio (i,avg) is the average ratio at the beginning of the oxidation period for all experiments. Fig. 4 shows that m/z 325 appears immediately and peaks after ~40 min of oxidation. In contrast, Δ increases throughout the oxidation period. We propose that under our conditions, at lower OH exposures, the siloxanol is formed first, and we start to see the influence of multigenerational chemistry on SiSOA composition as the disiloxanol is subsequently formed. This growth of the disiloxanol throughout the oxidation period suggests that later-generation siloxanols form to a greater extent at higher OH exposures, and our AMS spectra would trend towards those observed at higher OH exposures.[25,28,30]

Identification of the siloxanol as the major aerosol product and the disiloxanol as a minor one by AMS is consistent with analysis of the filter samples. Fig. 5 shows the average signal distribution of oVMS calculated using the combined gas-phase and particle-phase samples collected during E2–E4 and analyzed by UPLC-MS/MS. We combine gas- and particle-phase due to potential sampling artifacts described below. The predominant product was the siloxanol, accounting for 77% of the oVMS signal collected on the filter and over 99% of the oVMS collected on the PUF. There were minor contributions from later-generation siloxanols, including the di- and tri-siloxanol. Tetra- and pentasiloxanols were detected below the limit of quantification and tri-, tetra-, and penta-siloxanols were detected only in the particle-phase. D_4- and D_6-derived siloxanols were detected in a $D_5 : D_4 : D_6$ signal ratio of 100 : 1 : 0.4 suggesting that the D_4 and D_6 likely originated from impurities in the D_5 solution, as also suggested by the gas-phase CIMS measurements.[52] Fig. S10 presents the extracted chromatographic tracers for the identified D_4, D_5, and D_6 siloxanols, with the retention time (t_R) of the major peaks indicated by stars. In Fig. S11, the retention times of the major isomers are plotted against the number of Si atoms in their molecular formulas. These data reveal a consistent trend in which t_R increases with the addition of dimethyl-Si-O fragments due to the increased

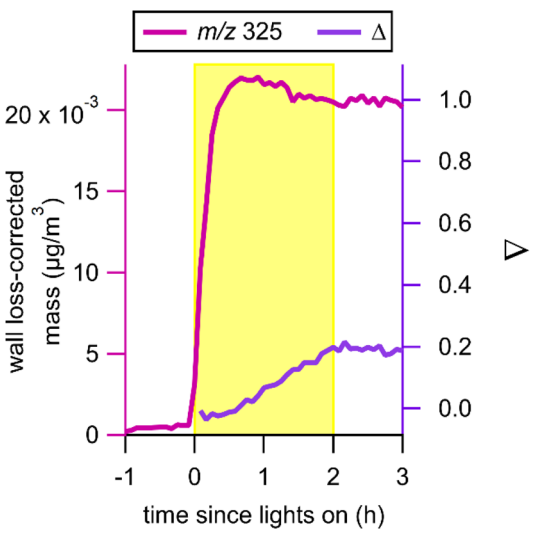

Fig. 4 Wall loss corrected AMS timeseries of m/z 325 (pink, left axis), a proxy for the siloxanol, and Δ (eqn (8); purple, right axis), a proxy for the disiloxanol, for experiment E7 with AS seed. Yellow shading indicates the lights on period. Measurements are averaged to 5 min time resolution.

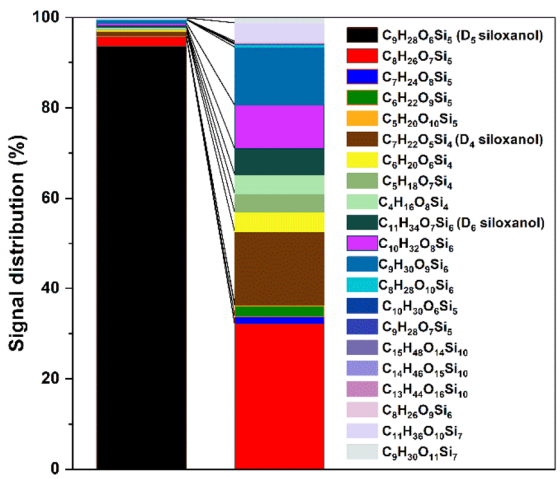

Fig. 5 The signal distribution of oVMS calculated using the combined gas-phase and particle-phase samples collected during the AS-seeded chamber experiments and analyzed by UPLC-MS/MS. See Table S6 for detailed descriptions of the molecular formulas.

molecular weight, while t_R decreases with the addition of OH groups due to enhanced hydrophilicity. These retention time patterns further enhance the confidence of the three siloxanol series identified.

The siloxanols were prominent in the field blank-subtracted, averaged full scan ESI (−) mass spectrum (Fig. S12; see peaks marked in blue). In addition to the molecular ions of siloxanols, fragment ions, isotopes, and adducts were observed as having matching retention times under the applied ESI (−) conditions (Table S5), in which collision energy was set to zero in order to promote molecular ion formation. The observed adducts have the same number of Si atoms as the identified siloxanols, with the addition of water ($m/z = [M] + 18.0338$) or formate ($m/z = [M] + 44.9982$), which are known to form under ESI (−) conditions.[53] While a prior study[29] proposed these m/z to be unique products, their co-elution with siloxanol molecular ions after reverse-phase chromatography suggests that they are instead variants of the major VMS siloxanol products. As shown in Fig. S13, extracted chromatographic tracers of the siloxanol and its silicon isotopologues ($C_9H_{28}O_6Si_4{}^{29}Si$, $C_9H_{28}O_6Si_3{}^{29}Si_2$, and $C_9H_{28}O_6Si_2{}^{29}Si_3$) as well as their adducts (water and formate) and fragments (m/z 355.0341, m/z 297.0456, m/z 223.0283) co-elute under the applied chromatographic conditions. The fragment ion at m/z 355.0341 is formed by the neutral loss of CH_4, m/z 297.0456 arises from the loss of a dimethyl Si–O fragment, and m/z 223.0283 results from the loss of two dimethyl Si–O fragments. Taken together, these data support that siloxanols are the major oxidation products of oVMS, with the first siloxanol product being the most abundant under our oxidation conditions. These results also suggest a fewer number of major oVMS products contribute to the ESI (−) mass spectrum than suggested by prior studies.[29]

Our UPLC-MS/MS method allowed us to identify several other compounds exclusively in the particle-phase with lower abundances (Table S6). A series of dimers formed by linking two siloxane rings through an oxygen atom, each containing additional siloxanol functional groups, were observed with the following compositions: $C_{15}H_{48}O_{14}Si_{10}$ (m/z 731.0658), $C_{14}H_{46}O_{15}Si_{10}$ (m/z 733.0451), and $C_{14}H_{46}O_{15}Si_{10}$ (m/z 735.0244). These dimers had very low relative abundance, accounting for 0.01% of the oVMS signal. Of these, $C_{15}H_{48}O_{14}Si_{10}$ could form by condensation between a disiloxanol and a trisiloxanol, resulting in linkage through an oxygen atom (Chart S1). Similarly, $C_{14}H_{46}O_{15}Si_{10}$ could form by coupling two trisiloxanols, while $C_{14}H_{46}O_{15}Si_{10}$ is more likely to result from the condensation of a trisiloxanol with a tetrasiloxanol. The detection of these dimers indicates that siloxanols undergo multiple oxidation steps and can condense to form higher-molecular weight compounds. Three other molecular formulas assigned as dimers contained 6–7 Si atoms (0.33% relative abundance) and are expected to have formed through reactions that involved fragmentation of the siloxane ring.

In addition to siloxanols, we observed a peak with the assigned molecular formula $C_{10}H_{30}O_6Si_5$ (m/z 385.0810, relative abundance of 0.001%), likely formed by the substitution of a methyl group by a silyl methanol group (Chart S1). Its retention time is slightly higher (~0.9 min) than that of the siloxanol,

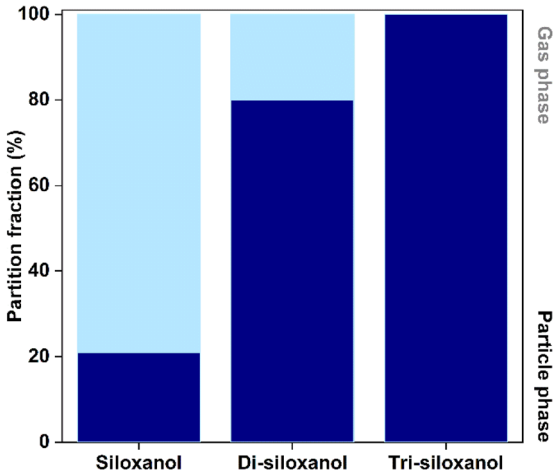

Fig. 6 The average partition fraction of D_5-derived siloxanols during the AS seeded chamber experiments. Note that particle fractions may be overestimated due to positive filter sampling artifacts.

which may be due to its lower hydrophilicity compared to the siloxanol functional group. Additionally, a compound with the molecular formula $C_9H_{28}O_7Si_5$ (m/z 387.0603, relative abundance of 0.005%) was detected at three distinct retention times and is believed to result from the replacement of one CH_3 group with a hydroxyl group and another with a silyl methanol group. The relatively low abundance of compounds containing silyl methanol functional groups is expected to result in part from their low ionization efficiency under the applied ESI (−) conditions, such that their true relative abundance may be significantly underestimated.

Gas-particle distributions of siloxanols. Latimer *et al.*[21] showed that the gas-particle partitioning of the siloxanol could be influenced by aerosol composition and varied with factors such as aerosol concentration, humidity, and temperature. Here we use our particulate and semi-volatile samples to estimate the gas-particle partitioning of major oVMS compounds in the presence of AS seed. Although this method provides valuable insights, it is limited in that it does not account for positive filter sampling artifacts (*i.e.* from adsorption of oVMS onto QFF) and may consequently over-estimate particle fractions. Despite this, the method is effective for identifying trends in gas-particle partitioning. As shown in Fig. 6, a clear trend emerged: the particle-phase concentration increased progressively with the addition of OH groups across the siloxanol series. Specifically, the particle fraction was 21% for the siloxanol, 80% for disiloxanol, and 100% for trisiloxanol. Furthermore, tetra- and pentasiloxanols were detected exclusively in the particle-phase, though their concentrations were below the limit of quantification. Dimers were also detected exclusively in the particle-phase, consistent with the CIMS measurements. This trend in partitioning provides direct evidence that D_5-derived aerosol tracers can partition into the particle-phase by forming more oxygenated compounds, particularly under urban plume conditions with 3–4 hours of atmospheric aging, with a concentrated D_5 loading.

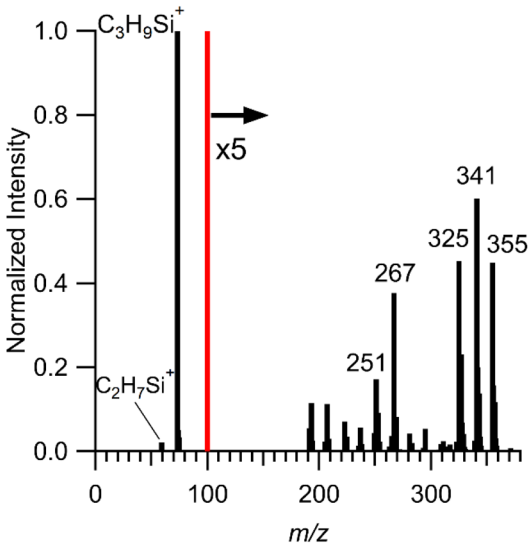

Fig. 7 Background-subtracted average AMS mass spectrum of SiSOA from experiment E9 with DOS seed. Spectrum is normalized to a $C_3H_9Si^+$ intensity of 1.

SiSOA formation and composition in DOS-seeded experiments

Fig. 7 shows an average mass spectrum of DOS-seeded SiSOA. The ions attributed to SiSOA were assigned using data from E11, where only DOS was oxidized, to account for the contribution of DOS and oxidized DOS to the mass spectrum. Below *m/z* 107 HR fitting was performed and only ions containing Si were attributed to SiSOA. Non-HR ions below *m/z* 190 were not included because of substantial DOS signal in that region. Ions at higher *m/z* values were included if they showed at least a factor of 4 enhancement compared to the DOS control experiment (Fig. S14). Some DOS ions may remain assigned to SiSOA, however we expect their contribution to be minor. The largest SiSOA signals all display the Si isotopic signature: the spectra are dominated by $C_3H_9Si^+$ and the groups of peaks at *m/z* 325, 341, and 355, with these peaks making up 80% of the signal at the end of experiment E10. Further reducing any potential overestimate of SiSOA is the fact that some ions associated with SiSOA (for instance CH_3^+, CHO^+, and CH_2O^+) are not attributed to SiSOA in this method. We note that a source attribution method such as positive matrix factorization is not possible with these measurements because the oxidation of DOS and the growth of SiSOA are highly correlated.

The DOS-SiSOA mass spectrum is striking in how it differs from the AS-SiSOA mass spectrum. A significant difference is the increase in the relative intensity of *m/z* 267 and 355 in the DOS spectrum. Additionally, *m/z* 341 is more intense than *m/z* 325 in the DOS experiments, the opposite of the AS experiments. While *m/z* 267 and 355 are present in the EI spectrum of D_5, these peaks increase when the lights turn on, not when D_5 is injected into the chamber. While we are unable to conclusively determine the identity of the new compound contributing to the SiSOA spectrum in the DOS experiments, we note that the gas-phase measurements indicated nearly identical gas-phase chemistry between the AS and DOS experiments. It is possible that there are other gas-phase oVMS species that are undetected by the CIMS, however Alton and Browne suggested that toluene CIMS was able to detect most of the first-generation oxidation products.[17] oVMS observed in other studies such as dimers[24,28,29] are unlikely to be formed in our experiments due to the lack of RO_2 + RO_2 chemistry. The differences in AMS spectra may be explained by another Si containing species, such as the formate ester, partitioning to the seed or it may indicate condensed-phase chemistry between oVMS and DOS oxidation products facilitated by the liquid nature of the DOS seed.

The DOS-seeded experiments also differ from the AS-seeded experiments in the temporal evolution of SiSOA in that SiSOA is continuously formed throughout the oxidation period (Fig. 8; see Fig. S15 for a side-by-side comparison). We note that the SiSOA in the DOS experiments was not corrected for wall loss; applying such corrections would be highly uncertain due to changing DOS density in response to oxidation. Normalization of the SiSOA timeseries to a DOS fragment ion is stable after the lights turn off, indicating that the SiSOA is in equilibrium with the gas-phase.

For similar OH exposures, the DOS-seeded experiment (E10) had a SiSOA yield ~3–10 times more than the AS-seeded experiments (Table S7). We did not observe any correlation between initial D_5 mixing ratio and amount of SiSOA formed (Table S7). Interestingly, growth of the disiloxanol is less important for DOS-seeded experiments (Fig. S16). Overall, these differences in identity and growth of SiSOA imply that different partitioning mechanisms are at play for each seed.

Modeling of SiSOA formation

AS-seeded experiments. Based on vapor pressure estimates, the effective saturation mass concentration (C^*) of the siloxanol

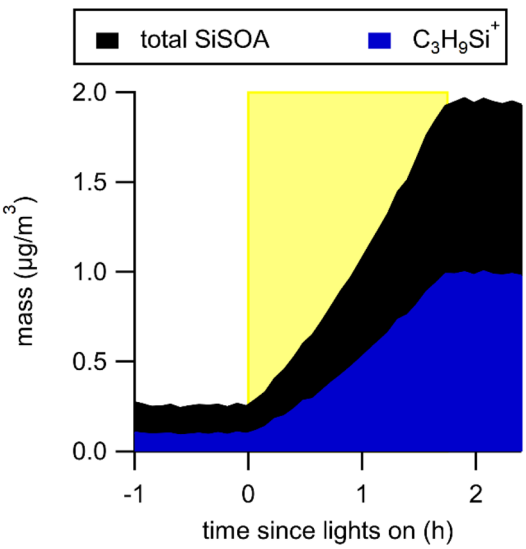

Fig. 8 Example AMS timeseries of SiSOA growth (not wall loss corrected) from experiment E9 with DOS seed. Yellow shading indicates when lights were on and oxidation was occurring. Measurements are averaged to 5 min time resolution.

and disiloxanol are 50 000 μg m^{-3} and 2600 μg m^{-3} respectively.[17] For the AS experiments, given an OA loading of 2.3 μg m^{-3} (background OA and SiSOA), the partitioning observed is inconsistent with absorptive partitioning, as is the observed SiSOA timeseries. To explain the presence of the siloxanol in the aerosol, we propose adsorption of the siloxanol onto the AS seed. The temporal behavior of the SiSOA concentration, stabilizing after ~40 min (Fig. 3) despite the continued increase of the gas-phase oxidation products (Fig. 1), is consistent with sorption sites becoming saturated and an equilibrium between adsorption and desorption being reached. The trend in *m/z* 325 (the marker for the siloxanol) and the trend in the marker for the disiloxanol (Δ) is consistent with desorption of the siloxanol followed by competitive adsorption of the disiloxanol. It is possible that the disiloxanol, which has an estimated vapor pressure ~20× lower than the siloxanol could partition *via* absorption and/or adsorption.[17]

To investigate the adsorption mechanism, we modeled SiSOA growth with AS seed assuming D_5 is oxidized to form the siloxanol and disiloxanol with C^* values of 50 000 μg m^{-3} and 2600 μg m^{-3} respectively.[17] With absorption only, there was negligible SOA formation. Upon adding adsorptive partitioning to the model, we were able to replicate the shape and amount of aerosol growth from our experiment. Competitive adsorption of the siloxanol and disiloxanol was modeled as in eqn (5) and (7). We constrained the accommodation coefficient, α_x, by calculating the adsorption for α_x values of 0.001 to 1 in steps of 0.001. We compared the total SiSOA formed to the measured AMS SiSOA signal to determine the best value for $\alpha_{s,0,X_i}$. We estimate the accommodation coefficient, $\alpha_{s,0,X_i}$, to be 0.215, for the estimated k_{off} of 0.03 s^{-1}. We use the same values of $\alpha_{s,0,X_i}$ and k_{off} for both the siloxanol and the disiloxanol to limit the number of variables.

Fig. 9 shows the results of adsorptive partitioning of the siloxanol and disiloxanol onto the AS seed compared to the measured SiSOA. Here we focus on the shape of the timeseries and thus normalize measured and modeled SiSOA, siloxanol, and disiloxanol to 1 at the end of the lights on period. The shape of the siloxanol growth generally agrees with the measured *m/z* 325 signal, with the increase and then slight decrease. The disiloxanol growth predicted by the model begins earlier than what was measured, therefore its k_{off} and α_x are likely different from the siloxanol. Because the amount of adsorbed siloxanol is slightly underestimated, the total SiSOA is also underestimated during oxidation. The SiSOA saturates the available sorption sites on the AS, as seen by the fractional surface coverage leveling off (Fig. S17). The model underpredicts the amount of SiSOA formed by approximately a factor of 2, however there are many uncertainties associated with assumptions in both the model and the measurements regarding the cross-section, monolayer, rate of desorption, treating the siloxanol and disiloxanol as having the same properties, and RIE of the SiSOA. We note that our measurements only constrain the relative values of $\alpha_{s,0,X_i}$ and k_{off}. If k_{off} is decreased by an order of magnitude to 0.003 s^{-1}, $\alpha_{s,0,X_i}$ is 0.024. For $\alpha_{s,0,X_i}$ to be 1, k_{off} would be 0.140. The ratios of k_{off} to α_x agree to within 10% of each other and the timeseries of the SiSOA, siloxanol, and disiloxanol are consistent between the three scenarios.

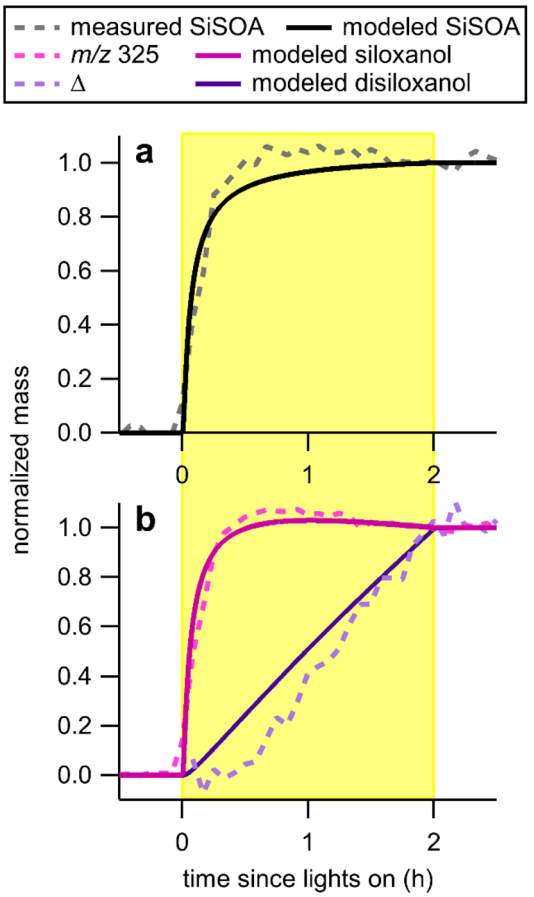

Fig. 9 Adsorption modeling timeseries for k_{off} of 0.03 s^{-1} and α_x of 0.215 compared to wall loss corrected AMS measurements. Timeseries are normalized to 1 when the lights turn off. The yellow shading represents when oxidation is occurring. Solid lines are modeled and dashed lines are measured. (a) Modeled SiSOA is the sum of the siloxanol and disiloxanol. (b) The modeled siloxanol is compared to *m/z* 325. The modeled disiloxanol is compared to Δ (eqn (8)). Note that the absolute amount of SiSOA is underestimated by a factor of 2 in the model.

To investigate whether the partitioning of the disiloxanol in the AS experiments was consistent with adsorption or a combination of adsorption and absorption, we used the SiSOA growth calculated by the adsorption model to rerun the absorption model in KinSim. In the base case, with 1.5 μg m^{-3} background OA, the SiSOA that was formed was negligible at only 0.007 μg m^{-3} (Fig. S18a). As a sensitivity test (case 1), we constrained the total OA to the background plus the modeled adsorbed SiSOA. This increased the SiSOA formed *via* absorption by only a small amount (total of 0.009 μg m^{-3} SiSOA) (Fig. S18b). We also investigated the sensitivity of the results to the assumed value of C^* by using a C^* of 1300 μg m^{-3} for the SiSOA (case 2; Fig. S18c). Because of the limited or negligible absorption to AS, we were unable to estimate a C^* from these experiments, therefore we used the C^* determined from the DOS experiments (described below). This too resulted in insufficient SiSOA (0.1 μg m^{-3}). In

all three cases (base case, case 1, and case 2), the model predicts that the SiSOA will increase throughout the experiment, a finding that is inconsistent with the AMS measurements.

In the base case and in case 1 (Fig. S18a and b), the model predicts that the disiloxanol will account for most of the SiSOA, a finding inconsistent with the offline measurements. Case 2 (Fig. S18c), in which C^* is assumed to be 1300 μg m^{-3} for both the siloxanol and the disiloxanol, shows more consistency with the offline measurements, although we note that it is unlikely both products have the same C^*. Overall, we conclude that adsorption is likely controlling the partitioning of the siloxanol. The partitioning mechanism of the disiloxanol remains inconclusive whether it is primarily adsorbing, absorbing or a combination.

Adsorption of the siloxanol as a mechanism for SiSOA formation is consistent with the work of Chandramouli and Kamens[20] who successfully simulated the siloxanol partitioning using an adsorption model. Although we did not observe partitioning of D_5 itself, previous work has observed uptake of D_5 onto AS.[54] That study investigated sorption of gas-phase D_5 onto non-atmospherically relevant levels of AS at 30% RH. The gas-phase D_5 decay showed an initial, fast uptake process, followed by a slower exponential decay, with multilayers of D_5 being formed.[54,55] Other studies also observed adsorption of D_5 onto mineral surfaces with multilayers being formed.[55,56] It was hypothesized that the multiple layers were due to surface chemistry of the D_5 because of the observed irreversibility of sorption.

In our experiments with AS, we observed an initial fast uptake process of the siloxanol, however the timeseries of our measurements suggests that if the siloxanol continues to adsorb, it is slower than the initial uptake. This observation also suggests that the monolayer does not serve as an absorbing seed for continued SiSOA growth. It is possible that intermolecular interactions between oVMS species are not conducive to absorption.

Multiple studies have observed siloxane oligomer adsorption onto particles flowing through conductive silicone tubing.[48,57,58] Relevant to our results, these past studies observed partitioning onto salt particles decrease as RH was increased.[48,57] D_5 partitioning onto mineral dust also decreased as RH increased.[55,56] A hypothesis for this was that water was taking up more of the available surface sorption sites. In contrast to VMS, the siloxanol could partition to water because of its hydroxyl group, however its estimated Henry's law coefficient[17] is still too low to make partitioning into aqueous aerosol likely. This is consistent with prior observations showing that the siloxanol partitioned to dust less as RH was increased.[21]

Previous OFR experiments investigating SiSOA yields observed that the addition of AS seed increased yields and altered the chemical composition of the SiSOA at OH exposures of $\sim 10^{11}$ molecules s cm^{-3} ([OH] $\approx 10^8$ molecules cm^{-3}).[24,25] A hypothesis for this effect was that the presence of seed enabled higher volatility products that formed earlier to partition to the aerosol. Our work showing that early-generation products are adsorbing to the AS seed is consistent with this hypothesis.

While absorption may be more important for later-generation oVMS, under low OH exposures and (mainly) one generation of oxidation chemistry with solid inorganic seed particles, adsorption of the siloxanol allows small amounts of SiSOA to form (~1% yield). For more substantial SiSOA growth, multiple generations of chemistry will be required to form products with lower vapor pressures.

While our experiments were closer to atmospheric conditions than many SiSOA experiments in the literature, the nature of running chamber experiments in batch mode means that D_5 and the oVMS are not continually diluted as they would be in the ambient atmosphere. To investigate the relevance of adsorption in the ambient atmosphere, we reran the adsorption model under the following condition: we approximated dilution in the atmosphere by setting the gas-phase siloxanol and disiloxanol concentrations to zero after the SiSOA reached its maximum, around 1 h into the oxidation period. The SiSOA completely evaporated after 4.6 min. This result suggests that the majority of the SiSOA formation on AS seed that we observed was an artifact of running the chamber experiments without dilution. We note that the evaporation timescale will depend upon assumptions of k_{off}. Our model only constrains the ratio of α_x to k_{off}. Future experiments investigating the evaporation behavior of SiSOA formed at low OH exposures are necessary to understand if adsorption onto salt aerosols will contribute to SiSOA in the ambient atmosphere.

DOS-seeded experiments. The timeseries of SiSOA during the DOS-seeded experiments is more consistent with absorptive partitioning as indicated by the continued growth of SiSOA throughout the oxidation period in both the shorter (~2 h) and longer (~5 h) experiments. The presence of the liquid organic aerosol seed allows the siloxanol and other oVMS to partition *via* absorption. To investigate the volatility of the SiSOA, we modeled SiSOA growth in the presence of the DOS seed as an absorptive process in KinSim assuming that one product is formed. We did not calculate adsorption. We determined a C^* value by calculating the absorption for values of 100 to 2000 μg m^{-3} in steps of 100 μg m^{-3}. We compared the calculated particle-phase siloxanol with the measured SiSOA to determine the best value for C^*. To replicate the amount and shape of SiSOA growth in experiment E9, a $C^*$of 1300 μg m^{-3} was required for the siloxanol (Fig. S19). While this is lower than the C^* of the siloxanol and disiloxanol calculated based on estimated vapor pressures, it is still characteristic of an intermediate volatility compound. We note that this C^* value would imply significant gas-wall partitioning (48% on the walls) based on parameterizations developed for partitioning of compounds containing carbon, hydrogen, and nitrogen atoms.[36] However our tubing delay experiment (Fig. S2) is inconsistent with 1300 μg m^{-3} being the correct C^* for gas-wall partitioning and instead suggests a value of $\sim 10^5$ μg m^{-3}. This finding suggests that the siloxanol undergoes different degrees of partitioning with DOS and Teflon.

Our estimated C^* is higher than the two-product fit for yields measured in Wu and Johnston[24] and Janechek *et al.*,[23] which predicted a yield of 0.82 for a C^* of 484 μg m^{-3}.[23] The aging-VBS model by Kang *et al.*[27] predicted that first-generation products

would be primarily (~90%) in the highest volatility bin ($C^* = 10\,000\ \mu g\ m^{-3}$) and ~9% in the bin with $C^* = 100\ \mu g\ m^{-3}$. With two days of aging ($OH_{exp} = 2.59 \times 10^{11}$ molecules s cm^{-3}), the product mass yield was ~67% in the highest volatility bin, ~19% in the second highest bin ($C^* = 1000\ \mu g\ m^{-3}$), and ~10% in the third highest bin.[27] Our estimate of 1300 $\mu g\ m^{-3}$ is more consistent with their result for two days of aging, although experiment E9 had an exposure equivalent to only half a day of aging.

Previous work investigating seed-dependent partitioning found that the siloxanol favorably partitioned (*via* adsorption) to inorganic dust whereas partitioning to combustion (wood, diesel, and coal) seed aerosol was minimal.[21] Here, we observe partitioning of the siloxanol *via* adsorption to inorganic salt aerosol and partitioning *via* absorption to liquid organic aerosol (DOS) seed. Across all the seeds in Latimer *et al.*[21] and this study, dust is the strongest sorbent, likely because of interactions between silicon atoms in the dust and the siloxanol. Our semi-quantitative estimates of yield suggest that more SiSOA was formed on DOS than in the combustion seed aerosol experiments of Latimer *et al.*[21] This difference is potentially explained by the liquid nature of the DOS seed allowing for absorption. In contrast, some fraction of the combustion particles was likely solid and thus absorption may not have been as favorable. Interestingly, Latimer *et al.*[21] observed that at higher RH the siloxanol partitioned more strongly to the combustion aerosol and attributed this effect to water increasing the polarity of the aerosol, thus increasing the solubility of the siloxanol. For dust, they observed decreased partitioning to the particle-phase at higher RH presumably due to competition for adsorption sites.

Conclusions

In order to understand the environmental impacts of D_5 emitted into the atmosphere, the fates of its oxidation products must be better constrained. Here we performed chamber experiments to investigate SOA formation from early-generation D_5 oxidation products. We measured gas-phase oxidation products consistent with only one generation of oxidation. No SiSOA was formed in the unseeded experiment, however low yields were observed with AS and DOS seed aerosol. The AS-seeded SiSOA was primarily composed of the siloxanol with small amounts of more oxidized products such as the di-siloxanol, while the DOS seed enabled absorption of other oVMS. Using our chromatography technique, we were able to identify water and formate siloxanol adducts that were previously thought to be distinct oVMS. We showed that D_5-derived aerosol tracers can partition into the particle-phase by forming more oxygenated compounds and to a lesser extent by condensing into dimers. The variety of analytical techniques we used enabled us to probe the evolution of SiSOA formation in its early stages and to analyze the SiSOA in bulk to retrieve more molecular information.

Our results indicate that for early-generation oVMS, adsorption is the primary SiSOA formation mechanism for solid inorganic seeds, and agree with previous work that for substantial SiSOA formation, multiple generations of D_5 oxidation chemistry will be required.[27] While we do not calculate SOA yields due to uncertainties in our D_5 measurements, our approximate yields for the AS-seeded experiments are ~≤1% (Table S7) and are consistent with previous chamber experiments at similar OH exposures.[26] An aspect not explored in our work was the influence of water content in the AS particles, which could influence SiSOA formation. Since VMS and their early-generation products have low Henry's coefficients, it is unlikely that early-generation oVMS would partition to an aqueous phase,[17] however the impact on surface adsorption is unclear. Future work should include investigation of adsorption dependence on RH. In contrast to the inorganic seed aerosol, the liquid organic seed exhibited absorptive partitioning and resulted in ~3–10 times more aerosol than the solid inorganic seed for similar OH exposures. It is possible that the phase of the seed plays a role in allowing absorption, therefore future work should probe SiSOA formation in the presence of varying organic seeds. Our work suggests that D_5-derived SOA is likely minor in the urban atmosphere, but more work needs to be done to characterize the seed dependence of SiSOA formation to predict SiSOA in the ambient atmosphere. Despite the low yields, SiSOA can still be used as a tracer for anthropogenic SOA sources given the lack of natural sources of VMS. SiSOA may be particularly useful as marker compounds when using offline detection methods such as those used in our study. Since the removal processes of D_5 and the siloxanol are slow, multiple generations of gas-phase chemistry will be required for removal from the atmosphere, with implications for deposition and long-range transport.

Author contributions

H. R. L.: investigation, formal analysis, methodology, software, validation, visualization, writing – original draft, writing – review and editing. J. N. M.: investigation, formal analysis, methodology, validation, visualization, writing – original draft, writing – review and editing. J. K. W.: investigation, formal analysis, methodology, validation, writing – original draft, writing – review and editing. C. O. S.: conceptualization, funding acquisition, project administration, supervision, writing – review and editing. E. A. S.: conceptualization, funding acquisition, project administration, supervision, writing – original draft, writing – review and editing. E. C. B.: conceptualization, formal analysis, funding acquisition, methodology, project administration, resources, software, supervision, writing – original draft, writing – review and editing.

Conflicts of interest

There are no conflicts to declare.

Data availability

Online data for this article are publicly available through the Index of Chamber Atmospheric Research in the United States website. The unseeded experiment is available at **https://icarus.ucdavis.edu/chambers/569/experimentSets/269**, the AS-

seeded experiments are available at https://icarus.ucdavis.edu/chambers/569/experimentSets/270, the DOS-seeded experiments are available at https://icarus.ucdavis.edu/chambers/569/experimentSets/271, and the DOS-only oxidation experiment is available at https://icarus.ucdavis.edu/chambers/569/experimentSets/272.

Supplementary information: chemical structures, tubing delays, D_5 background discussion, modeling, doubly charged ions, offline results. See DOI: https://doi.org/10.1039/d5ea00063g.

Acknowledgements

This research was supported by the National Science Foundation under Grant AGS-2029017 and AGS-2028764, and CHE-1919422. Any opinions, findings, and conclusions or recommendations expressed in this material are those of the author(s) and do not necessarily reflect the views of the National Science Foundation. The authors thank Saeideh Mohammadi, Carlos Gutierrez, Jim Hall, Douglas Day, Anne Handschy, Dongwook Kim, Seonsik Yun, and Pedro Campuzano-Jost for their assistance with operating the chamber and instruments during the experiments. We also thank Lynn Teesch and Vic Parcell for their assistance with and training in the University of Iowa High Resolution Mass Spectrometry Facility (HRMSF) and Alexandra Glennon for helping with the PUF extractions.

Notes and references

1 C. Rücker and K. Kümmerer, Environmental Chemistry of Organosiloxanes, *Chem. Rev.*, 2015, **115**, 466–524.
2 S. Genualdi, T. Harner, Y. Cheng, M. MacLeod, K. M. Hansen, R. van Egmond, M. Shoeib and S. C. Lee, Global Distribution of Linear and Cyclic Volatile Methyl Siloxanes in Air, *Environ. Sci. Technol.*, 2011, **45**, 3349–3354.
3 D. Mackay, C. E. Cowan-Ellsberry, D. E. Powell, K. B. Woodburn, S. Xu, G. E. Kozerski and J. Kim, Decamethylcyclopentasiloxane (D5) environmental sources, fate, transport, and routes of exposure, *Environ. Toxicol. Chem.*, 2015, **34**, 2689–2702.
4 N. J. Janechek, K. M. Hansen and C. O. Stanier, Comprehensive atmospheric modeling of reactive cyclic siloxanes and their oxidation products, *Atmos. Chem. Phys.*, 2017, **17**, 8357–8370.
5 C. E. Brunet, R. F. Marek, C. O. Stanier and K. C. Hornbuckle, Concentrations of Volatile Methyl Siloxanes in New York City Reflect Emissions from Personal Care and Industrial Use, *Environ. Sci. Technol.*, 2024, **58**, 8835–8845.
6 S. Xu and F. Wania, Chemical fate, latitudinal distribution and long-range transport of cyclic volatile methylsiloxanes in the global environment: A modeling assessment, *Chemosphere*, 2013, **93**, 835–843.
7 R. He, K. Fang, J. Qian, S. Duan, F. Jiang, Y. Lu, Z. Dong, L. Xu, W. Gu and S. Tang, A Review of Contamination Status and Health Risk Assessment of Volatile Methylsiloxanes in Environmental Matrices, *Environ. Health*, 2025, **3**, 837–853.
8 N. J. Janechek, K. M. Hansen and C. O. Stanier, Comprehensive atmospheric modeling of reactive cyclic siloxanes and their oxidation products, *Atmos. Chem. Phys.*, 2017, **17**, 8357–8370.
9 M. M. Coggon, B. C. McDonald, A. Vlasenko, P. R. Veres, F. Bernard, A. R. Koss, B. Yuan, J. B. Gilman, J. Peischl, K. C. Aikin, J. DuRant, C. Warneke, S.-M. Li and J. A. de Gouw, Diurnal Variability and Emission Pattern of Decamethylcyclopentasiloxane (D_5) from the Application of Personal Care Products in Two North American Cities, *Environ. Sci. Technol.*, 2018, **52**, 5610–5618.
10 G. I. Gkatzelis, M. M. Coggon, B. C. McDonald, J. Peischl, K. C. Aikin, J. B. Gilman, M. Trainer and C. Warneke, Identifying Volatile Chemical Product Tracer Compounds in U.S. Cities, *Environ. Sci. Technol.*, 2021, **55**, 188–199.
11 D. Brooke, M. Crookes, D. Gray and S. Robertson, *Environmental Risk Assessment Report: Decamethylcyclopentasiloxane*, Environment Agency, Bristol, 2009.
12 M. W. Lieberman, E. D. Lykissa, R. Barrios, C. N. Ou, G. Kala and S. V. Kala, Cyclosiloxanes produce fatal liver and lung damage in mice, *Environ. Health Perspect.*, 1999, **107**, 161–165.
13 L. Xu, Y. Shi, N. Liu and Y. Cai, Methyl siloxanes in environmental matrices and human plasma/fat from both general industries and residential areas in China, *Sci. Total Environ.*, 2015, **505**, 454–463.
14 M. S. McLachlan and F. Wania, Are Cyclic Volatile Methylsiloxanes POPs? For Rigorous Science in Regulatory Decision Making, *Environ. Sci. Technol.*, 2024, **58**, 8607–8609.
15 R. Atkinson, E. C. Tuazon, E. S. C. Kwok, J. Arey, S. M. Aschmann and I. Bridier, Kinetics and Products of the Gas-phase Reactions of $(CH_3)_3SiCH_2OH$, $(CH_3)_3SiOSi(CH_3)_3$ and $(CD_3)_3SiOSi(CD_3)_3$ with Cl Atoms and OH Radicals, *J. Chem. Soc., Faraday Trans.*, 1995, **91**, 3033–3039.
16 M. W. Alton and E. C. Browne, Atmospheric Chemistry of Volatile Methyl Siloxanes: Kinetics and Products of Oxidation by OH Radicals and Cl Atoms, *Environ. Sci. Technol.*, 2020, **54**, 5992–5999.
17 M. W. Alton and E. C. Browne, Atmospheric Degradation of Cyclic Volatile Methyl Siloxanes: Radical Chemistry and Oxidation Products, *ACS Environ. Au*, 2022, **2**, 263–274.
18 A. Milani, I. M. Al-Naiema and E. A. Stone, Detection of a secondary organic aerosol tracer derived from personal care products, *Atmos. Environ.*, 2021, **246**, 118078.
19 J. N. Meepage, J. K. Welker, C. M. Meyer, S. Mohammadi, C. O. Stanier and E. A. Stone, Advances in the Separation and Detection of Secondary Organic Aerosol Produced by Decamethylcyclopentasiloxane (D_5) in Laboratory-Generated and Ambient Aerosol, *ACS EST Air*, 2024, **1**, 365–375.
20 B. Chandramouli and R. M. Kamens, The photochemical formation and gas–particle partitioning of oxidation products of decamethyl cyclopentasiloxane and decamethyl tetrasiloxane in the atmosphere, *Atmos. Environ.*, 2001, **35**, 87–95.

21 H. K. Latimer, R. M. Kamens and G. Chandra, The atmospheric partitioning of decamethylcyclopentasiloxane(D5) and 1-hydroxynonamethylcyclopentasiloxane(D4TOH) on different types of atmospheric particles, *Chemosphere*, 1998, **36**, 2401–2414.

22 J. Wu, N. Brun, J. M. González-Sánchez, B. R'Mili, B. Temime Roussel, S. Ravier, J.-L. Clément and A. Monod, Substantial organic impurities at the surface of synthetic ammonium sulfate particles, *Atmos. Meas. Tech.*, 2022, **15**, 3859–3874.

23 N. J. Janechek, R. F. Marek, N. Bryngelson, A. Singh, R. L. Bullard, W. H. Brune and C. O. Stanier, Physical properties of secondary photochemical aerosol from OH oxidation of a cyclic siloxane, *Atmos. Chem. Phys.*, 2019, **19**, 1649–1664.

24 Y. Wu and M. V. Johnston, Aerosol Formation from OH Oxidation of the Volatile Cyclic Methyl Siloxane (cVMS) Decamethylcyclopentasiloxane, *Environ. Sci. Technol.*, 2017, **51**, 4445–4451.

25 C. Han, H. Yang, K. Li, P. Lee, J. Liggio, A. Leithead and S.-M. Li, Secondary organic aerosols from OH oxidation of cyclic volatile methyl siloxanes as an important Si source in the atmosphere, *Atmos. Chem. Phys.*, 2022, **22**, 10827–10839.

26 S. M. Charan, Y. Huang, R. S. Buenconsejo, Q. Li, D. R. Cocker III and J. H. Seinfeld, Secondary organic aerosol formation from the oxidation of decamethylcyclopentasiloxane at atmospherically relevant OH concentrations, *Atmos. Chem. Phys.*, 2022, **22**, 917–928.

27 H. G. Kang, Y. Chen, Y. Park, T. Berkemeier and H. Kim, Volatile oxidation products and secondary organosiloxane aerosol from D_5 + OH at varying OH exposures, *Atmos. Chem. Phys.*, 2023, **23**, 14307–14323.

28 A. M. Avery, M. W. Alton, M. R. Canagaratna, J. E. Krechmer, D. T. Sueper, N. Bhattacharyya, L. Hildebrandt Ruiz, W. H. Brune and A. T. Lambe, Comparison of the Yield and Chemical Composition of Secondary Organic Aerosol Generated from the OH and Cl Oxidation of Decamethylcyclopentasiloxane, *ACS Earth Space Chem.*, 2023, **7**, 218–229.

29 Y. Wu and M. V. Johnston, Molecular Characterization of Secondary Aerosol from Oxidation of Cyclic Methylsiloxanes, *J. Am. Soc. Mass Spectrom.*, 2016, **27**, 402–409.

30 Y. Chen, Y. Park, H. G. Kang, J. Jeong and H. Kim, Chemical characterization and formation of secondary organosiloxane aerosol (SOSiA) from OH oxidation of decamethylcyclopentasiloxane, *Environ. Sci.: Atmos.*, 2023, **3**, 662–671.

31 Z. Peng, J. Lee-Taylor, J. J. Orlando, G. S. Tyndall and J. L. Jimenez, Organic peroxy radical chemistry in oxidation flow reactors and environmental chambers and their atmospheric relevance, *Atmos. Chem. Phys.*, 2019, **19**, 813–834.

32 J. E. Krechmer, D. A. Day, P. J. Ziemann and J. L. Jimenez, Direct Measurements of Gas/Particle Partitioning and Mass Accommodation Coefficients in Environmental Chambers, *Environ. Sci. Technol.*, 2017, **51**, 11867–11875.

33 M. R. Canagaratna, J. T. Jayne, J. L. Jimenez, J. D. Allan, M. R. Alfarra, Q. Zhang, T. B. Onasch, F. Drewnick, H. Coe, A. Middlebrook, A. Delia, L. R. Williams, A. M. Trimborn, M. J. Northway, P. F. DeCarlo, C. E. Kolb, P. Davidovits and D. R. Worsnop, Chemical and microphysical characterization of ambient aerosols with the aerodyne aerosol mass spectrometer, *Mass Spectrom. Rev.*, 2007, **26**, 185–222.

34 A. Shahar, in *Encyclopedia of Geochemistry: A Comprehensive Reference Source on the Chemistry of the Earth*, ed. W. M. White, Springer International Publishing, Cham, 2016, pp. 1–4.

35 D. Pagonis, J. E. Krechmer, J. de Gouw, J. L. Jimenez and P. J. Ziemann, Effects of gas–wall partitioning in Teflon tubing and instrumentation on time-resolved measurements of gas-phase organic compounds, *Atmos. Meas. Tech.*, 2017, **10**, 4687–4696.

36 J. E. Krechmer, D. Pagonis, P. J. Ziemann and J. L. Jimenez, Quantification of Gas-Wall Partitioning in Teflon Environmental Chambers Using Rapid Bursts of Low-Volatility Oxidized Species Generated in Situ, *Environ. Sci. Technol.*, 2016, **50**, 5757–5765.

37 F. Bernard and J. B. Burkholder, Rate coefficients for the gas-phase reaction of OH radicals with the L_4 , L_5 , D_5 , and D_6 permethylsiloxanes, *Int. J. Chem. Kinet.*, 2025, **57**, 199–212.

38 I. M. Al-Naiema and E. A. Stone, Evaluation of anthropogenic secondary organic aerosol tracers from aromatic hydrocarbons, *Atmos. Chem. Phys.*, 2017, **17**, 2053–2065.

39 Z. Peng and J. L. Jimenez, KinSim: A Research-Grade, User-Friendly, Visual Kinetics Simulator for Chemical-Kinetics and Environmental-Chemistry Teaching, *J. Chem. Educ.*, 2019, **96**, 806–811.

40 R. Atkinson, D. L. Baulch, R. A. Cox, J. N. Crowley, R. F. Hampson, R. G. Hynes, M. E. Jenkin, M. J. Rossi and J. Troe, Evaluated kinetic and photochemical data for atmospheric chemistry: Volume I - gas phase reactions of O_x, HO_x, NO_x and SO_x species, *Atmos. Chem. Phys.*, 2004, **4**, 1461–1738.

41 R. Atkinson, D. L. Baulch, R. A. Cox, J. N. Crowley, R. F. Hampson, R. G. Hynes, M. E. Jenkin, M. J. Rossi and J. Troe, Evaluated kinetic and photochemical data for atmospheric chemistry: Volume III – gas phase reactions of inorganic halogens, *Atmos. Chem. Phys.*, 2007, **7**, 981–1191.

42 P. J. Ziemann and R. Atkinson, Kinetics, products, and mechanisms of secondary organic aerosol formation, *Chem. Soc. Rev.*, 2012, **41**, 6582–6605.

43 C. Fittschen, The reaction of peroxy radicals with OH radicals, *Chem. Phys. Lett.*, 2019, **725**, 102–108.

44 M. W. Alton, V. L. Johnson, S. Sharma and E. C. Browne, Volatile Methyl Siloxane Atmospheric Oxidation Mechanism from a Theoretical Perspective—How is the Siloxanol Formed?, *J. Phys. Chem. A*, 2023, **127**, 10233–10242.

45 U. Pöschl, Y. Rudich and M. Ammann, Kinetic model framework for aerosol and cloud surface chemistry and gas-particle interactions – Part 1: General equations,

parameters, and terminology, *Atmos. Chem. Phys.*, 2007, **7**, 5989–6023.

46 M. Ammann and U. Pöschl, Kinetic model framework for aerosol and cloud surface chemistry and gas-particle interactions – Part 2: Exemplary practical applications and numerical simulations, *Atmos. Chem. Phys.*, 2007, **7**, 6025–6045.

47 Hazardous Substances Data Bank, **https://pubchem.ncbi.nlm.nih.gov/compound/decamethylcyclopentasiloxane#section=Density**, accessed 2 May 2025.

48 M. T. Timko, Z. Yu, J. Kroll, J. T. Jayne, D. R. Worsnop, R. C. Miake-Lye, T. B. Onasch, D. Liscinsky, T. W. Kirchstetter, H. Destaillats, A. L. Holder, J. D. Smith and K. R. Wilson, Sampling Artifacts from Conductive Silicone Tubing, *Aerosol Sci. Technol.*, 2009, **43**, 855–865.

49 NIST Chemistry WebBook, **https://webbook.nist.gov/cgi/cbook.cgi?ID=C541026&Units=SI&Mask=200#Mass-Spec**, accessed 26 February 2025.

50 V. Yu. Orlov, N. S. Nametkin, L. E. Gusel'nikov and T. H. Islamov, Electron-impact fragmentation of cyclocarbosiloxanes, *Org. Mass Spectrom.*, 1970, **4**, 195–201.

51 B. M. Matthew, A. M. Middlebrook and T. B. Onasch, Collection Efficiencies in an Aerodyne Aerosol Mass Spectrometer as a Function of Particle Phase for Laboratory Generated Aerosols, *Aerosol Sci. Technol.*, 2008, **42**, 884–898.

52 R. Gerhards, R. M. Seston, G. E. Kozerski, D. A. McNett, T. Boehmer, J. A. Durham and S. Xu, Basic considerations to minimize bias in collection and analysis of volatile methyl siloxanes in environmental samples, *Sci. Total Environ.*, 2022, **851**, 158275.

53 H. Tong, D. Bell, K. Tabei and M. M. Siegel, Automated data massaging, interpretation, and e-mailing modules for high throughput open access mass spectrometry, *J. Am. Soc. Mass Spectrom.*, 1999, **10**, 1174–1187.

54 J. Kim and S. Xu, Sorption and desorption kinetics and isotherms of volatile methylsiloxanes with atmospheric aerosols, *Chemosphere*, 2016, **144**, 555–563.

55 J. G. Navea, S. Xu, C. O. Stanier, M. A. Young and V. H. Grassian, Heterogeneous uptake of octamethylcyclotetrasiloxane (D_4) and decamethylcyclopentasiloxane (D_5) onto mineral dust aerosol under variable RH conditions, *Atmos. Environ.*, 2009, **43**, 4060–4069.

56 J. G. Navea, S. Xu, C. O. Stanier, M. A. Young and V. H. Grassian, Effect of Ozone and Relative Humidity on the Heterogeneous Uptake of Octamethylcyclotetrasiloxane and Decamethylcyclopentasiloxane on Model Mineral Dust Aerosol Components, *J. Phys. Chem. A*, 2009, **113**, 7030–7038.

57 Y. Yu, M. Liz Alexander, V. Perraud, E. A. Bruns, S. N. Johnson, M. J. Ezell and B. J. Finlayson-Pitts, Contamination from electrically conductive silicone tubing during aerosol chemical analysis, *Atmos. Environ.*, 2009, **43**, 2836–2839.

58 J. Schneider, S. Weimer, F. Drewnick, S. Borrmann, G. Helas, P. Gwaze, O. Schmid, M. O. Andreae and U. Kirchner, Mass spectrometric analysis and aerodynamic properties of various types of combustion-related aerosol particles, *Int. J. Mass Spectrom.*, 2006, **258**, 37–49.